Analytical Evaluation of the Peak-to-peak Ripple Current in the Filter Inductor for a Space Vector Modulated Grid-tied VSI

Saurabh Tewari
Dynapower Company LLC
Email: tewar007@umn.edu

Kaushik Basu
Dynapower Company LLC
Email: kbasu@dynapower.com

Apurva Somani
Dynapower Company LLC
Email: asomani@dynapower.com

***Abstract*—Two level voltage source inverters are extensively employed to integrate renewable energy sources and storage with the grid. The output voltage of the inverter, modulated with conventional space vector PWM, contains switching frequency components along with the desired grid frequency component. Usually a filter inductor or an LCL filter is used to remove these high frequency components resulting in low THD in the grid current. Either all, or a majority of the higher frequency components of the inverter output voltage appear across the inverter-side filter inductance, resulting in ripple current through it. This paper presents an analytical estimation of the peak-to-peak ripple current as a function of the modulation index, essential for the design of the filter. Simulation results confirm the analytical prediction of the ripple current.**

***Index Terms*—Peak-to-peak ripple current, grid-tied inverter, VSI, LCL filter, SVPWM**

I. Introduction

GRID-tied two level voltage source inverters (VSI) have become a standard solution for the integration of renewable energy sources like photovoltaic, and energy storage to the grid [1], [2]. The power rating of these converters ranges from a few kilowatts to several megawatts. The grid-tied VSI is switched to control the exchange of the active and reactive power with the grid. The pulse width modulated (PWM) output voltage of the VSI contains switching frequency harmonics along with the desired fundamental component at the grid frequency. These harmonics have been extensively studied in the context of motor drives [3].

An inductor connecting the inverter output to the grid is the simplest filter to attenuate these harmonics. However, a purely inductive filter alone proves bulky. Typically an LCL filter is used to remove these high frequency harmonics [4] in grid-tied applications. Due to very low THD in the grid current ($< 5\%$ per IEEE 519), it is reasonable to assume that the voltage across the capacitor of the LCL filter is close to sinusoidal at the grid frequency. This implies that most of the switching components of the voltage generated by the VSI appear across the inverter side inductance of the LCL filter resulting in substantial ripple current through it.

For the design of the inverter side filter inductance it is essential to estimate the peak-to-peak ripple current. Again assuming low THD in the grid current, most of the ripple current flows through the capacitance of the LCL filter. So prediction of the peak-to-peak ripple component present in the output line currents of the VSI is also important for the design of the filter capacitance. An estimate of the maximum peak-to-peak current ripple over a complete range of modulation index is known in the literature [5]. Some authors consider this as an approximate estimate as no analysis has been presented to validate it [4], [5].

This paper confirms this limit through a detailed analysis of the switching voltage that appears across the inverter side filter inductance, when modulated with conventional space vector PWM. This paper also provides a closed form analytical expression of the peak-to-peak ripple current as a function of the modulation index, essential for the filter design. The entire system has been simulated in MATLAB and presented simulation results verify the analysis of the peak-to-peak ripple current.

II. Analysis

This section presents a detailed analysis of the peak-to-peak ripple in the output current of the inverter. As argued in the Introduction, under low grid current THD, the voltage across the capacitance of the LCL filter can be approximated as the grid voltage. Therefore, the analysis conducted for a purely inductive, first-order filter will be valid for an LCL filter as well. Fig. 1 shows this simplified configuration considered in this research, where L is the inverter side filter inductance. The inverter, switching at a frequency f_{sw}, modulates a DC voltage, V_{DC}, connected across the terminals P, N to generate voltages $v_{aN}, \ldots$ at its output terminals. These voltages can be written as the sum of a low-frequency component (averaged over a carrier cycle of period $T_s = 1/f_{\text{sw}}$) and a high-frequency (switching) component: The inductors $L_{a,b,c}$ limit the ripple current entering the grid at the points a', b', c'. The complex

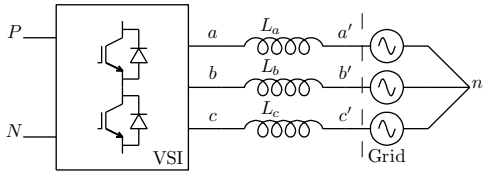

Fig. 1. System diagram

978-1-4799-6373-7/14/$31.00 ©2014 IEEE

power transfer is controlled by adjusting a) the phase angle δ between the synthesized voltages ($\overline{v}_{an},\ldots$) and the grid voltages $v'_{an},\ldots$; and b) the amplitude of the synthesized voltage.

$$v_{iN} = \overline{v}_{iN} + \tilde{v}_{iN} \qquad i \in \{a,b,c\} \tag{1}$$

$$= \overline{v}_{in} + \tilde{v}_{in} + \underbrace{\overline{v}_{nN} + \tilde{v}_{nN}}_{:=v_{\mathrm{CM}}} \tag{2}$$

$$v_{\mathrm{CM}} = \frac{v_{aN} + v_{bN} + v_{cN}}{3} \tag{3}$$

Let ω be the grid voltage angular frequency. Further, let

$$\begin{aligned} \overline{v}_{an} &= mV_{DC}\cos(\omega t + \delta) \\ \overline{v}_{bn} &= mV_{DC}\cos(\omega t - 2\pi/3 + \delta) \\ \overline{v}_{cn} &= mV_{DC}\cos(\omega t + 2\pi/3 + \delta) \end{aligned} \tag{4}$$

where m is the modulation index. Fig. 2 shows the inverter AC output currents for a 480 V, 60 Hz grid with $L = 1\,\mathrm{mH}$ at $m = 0.55, mV_{DC} = \widehat{v}'_{an}, \delta = \pi/24, f_{\mathrm{sw}} = 6\,\mathrm{kHz}$

Since the common-mode path is open, no current flows due to the common-mode voltage v_{CM}: to calculate the current flowing through the inductors, it is sufficient to look at the voltages $\overline{v}_{in}+\tilde{v}_{in}$ for $i \in \{a,b,c\}$. Furthermore, the low frequency component does not contribute to the peak-to-peak ripple by definition (peak-to-peak ripple is the switching ripple riding on the low frequency component). For calculating the peak-to-peak ripple, the high-frequency component alone of the voltage across the inductor needs to be examined. Therefore, the analysis could be done at no-load ($\delta = 0, mV_{DC} = \widehat{v}'_{an}$).

Let $\alpha \in [0, 2\pi)$ be the phase angle of the voltage synthesized by the inverter: $\alpha = \omega t + \delta$. Let sector-I be $\alpha : \alpha \in [0, \pi/3)$. Fig. 3 shows the voltages v_{bn} and v_{an}, and their low frequency components $\overline{v}_{bn}, \overline{v}_{an}$ at different points within sector-I at no-load ($\delta = 0, mV_{DC} = \widehat{v}'_{an}$). Currents evolve differently depending upon the the value of the fundamental component of the voltage. Therefore it is required to consider multiple cases shown in Figs. 3(a)–(d), and identify the path along which maximum Volt-seconds are accumulated (ΔVs) for each of these cases, where Volt-seconds (Vs) is the integral of the voltage across the inductor.

A. *Sector-I,* $\overline{v}_{bn} \lessgtr 0$

First consider the case $\overline{v}_{bn} < 0$ shown in Fig. 3(a). By symmetry of SVPWM, the accumulated Volt-seconds are reset

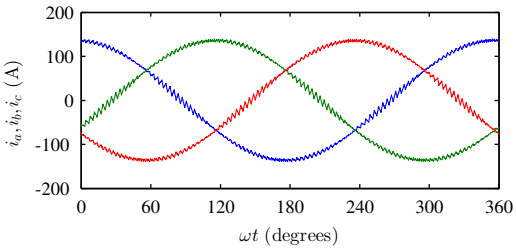

Fig. 2. Inverter output currents for a 480 V, 60 Hz system with $L = 1\,\mathrm{mH}$ at $m = 0.55, mV_{DC} = \widehat{v}'_{an}, \delta = \pi/24, f_{\mathrm{sw}} = 6\,\mathrm{kHz}$ (power flows from the inverter to the grid)

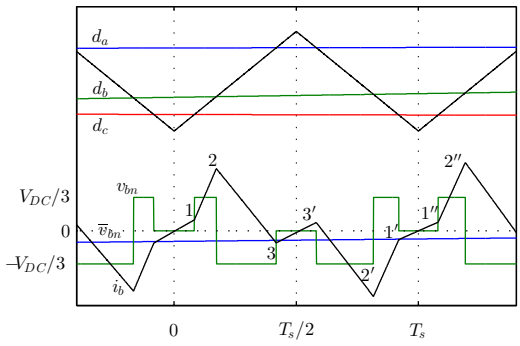

(a) $v_{bn}, \overline{v}_{bn}, i_b$ for $\overline{v}_{bn} < 0$

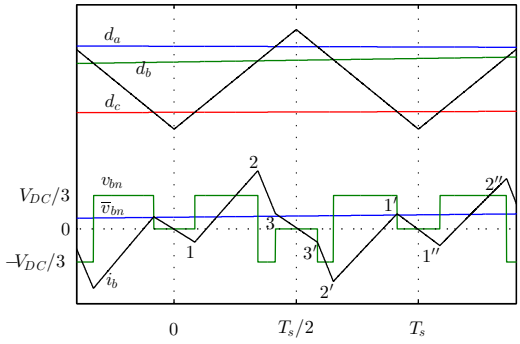

(b) $v_{bn}, \overline{v}_{bn}, i_b$ for $\overline{v}_{bn} > 0$

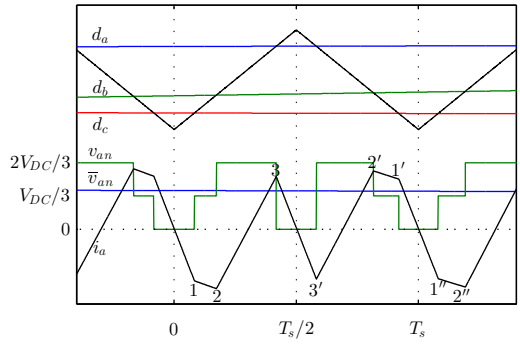

(c) $v_{an}, \overline{v}_{an}, i_a$ for $\overline{v}_{an} > V_{DC}/3$

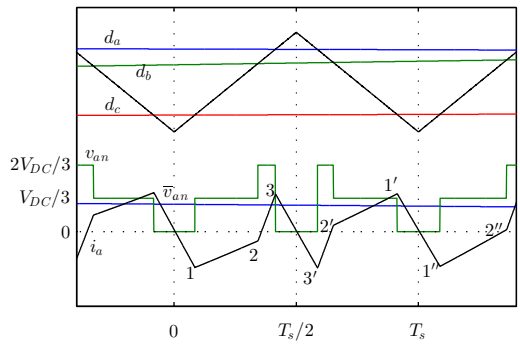

(d) $v_{an}, \overline{v}_{an}, i_a$ for $\overline{v}_{an} < V_{DC}/3$

Fig. 3. Switching voltage synthesized by the inverter along with its switching cycle average and the current through the inductor at no-load for phases a and b in the first sector ($\alpha \in [0, \pi/3)$)

to zero every half cycle, at the peaks and the valleys of the triangular carrier. Furthermore, the ripple current waveform can be considered periodic between consecutive switching cycles (since the line frequency is much lower than the switching frequency).

Due to the symmetric placement of the zero-vector and the active vectors, $|\Delta \mathrm{Vs}|$ is maximized along one of the three paths, $1-1', 2-2'$, and $3-3'$. Furthermore, $\mathrm{Vs}(1), \mathrm{Vs}(1'), \mathrm{Vs}(3)$, and $\mathrm{Vs}(3')$, are all equal in magnitude. It is then seen in Fig. 3(a) that the maximum Vs are accumulated along the path $2'-2''$, which is also equal in magnitude to $2-2'$.

Let d_a be the duty ratio of the top switch of phase leg a of the inverter. d_b, d_c can be defined similarly for the other legs.

$$d_{\mathrm{com}} := \frac{1}{2} + \frac{1}{2V_{DC}}(-\max(\overline{v}_{an}, \overline{v}_{bn}, \overline{v}_{cn}) - \min(\overline{v}_{an}, \overline{v}_{bn}, \overline{v}_{cn})) \quad (5)$$

$$\begin{aligned} d_a &= \frac{\overline{v}_{an}}{V_{DC}} + d_{\mathrm{com}} \\ d_b &= \frac{\overline{v}_{bn}}{V_{DC}} + d_{\mathrm{com}} \\ d_c &= \frac{\overline{v}_{cn}}{V_{DC}} + d_{\mathrm{com}} \end{aligned} \quad (6)$$

From Fig. 3(a) along $2-2'$

$$|\Delta \mathrm{Vs}|_{2-2'} = \left(\frac{V_{DC}}{3} + \overline{v}_{bn}\right) \times \frac{d_a - d_b}{f_{\mathrm{sw}}} + \overline{v}_{bn}\frac{1-d_a}{f_{\mathrm{sw}}} \quad (7)$$

After substituting the expressions for $d_a, \ldots$ and $\overline{v}_{bn}$, and normalizing $\Delta \mathrm{Vs}$ by V_{DC}/f_{sw}, (7) yields (10). Furthermore, the path $2-2'$ is also the path of maximum Volt-seconds for $\overline{v}_{bn} > 0$, shown in Fig. 3(b), and (7) and (10) apply to this case as well.

B. Sector-I, $\overline{v}_{an} > V_{DC}/3$

It is seen from Fig. 3(c) that the maximum Volt-seconds are accrued along the path $2-2'$

$$|\Delta \mathrm{Vs}|_{2-2'} = \left(\frac{2V_{DC}}{3} - \overline{v}_{an}\right) \times \left(\frac{d_a - d_b}{f_{\mathrm{sw}}}\right) - \overline{v}_{an}\left(\frac{1-d_a}{f_{\mathrm{sw}}}\right) \quad (8)$$

After appropriate substitution and normalization by V_{DC}/f_{sw}, (8) yields (11)

C. Sector-I, $\overline{v}_{an} < V_{DC}/3$

This case is shown in Fig. 3(d). Using similar arguments as above, it can be shown that the maximum Volt-seconds are accumulated along the path $3-3'$ and have a magnitude defined below:

$$|\Delta \mathrm{Vs}|_{3-3'} = (1-d_a)\frac{\overline{v}_{an}}{f_{\mathrm{sw}}} \quad (9)$$

After appropriate substitution and normalization by V_{DC}/f_{sw}, (9) yields (12)

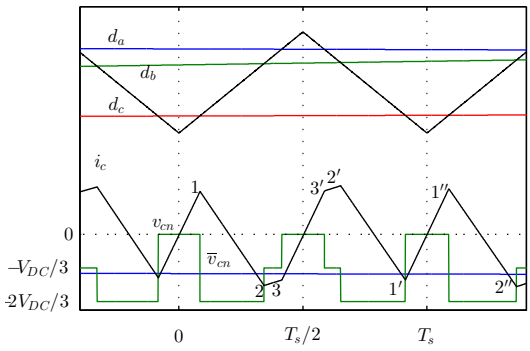

Fig. 4. Switching voltage synthesized by the inverter along with its switching cycle average and the current through the inductor at no-load for phase c in the first sector ($\alpha \in [0, \pi/3)$) with $\overline{v}_{cn} < -V_{DC}/3$

D. Sector-I, phase c

Fig. 4 shows the duty ratios, voltages, and current for phase c at no-load under the same conditions as Fig. 3. $\overline{v}_{cn}$ is lower than $-V_{DC}/3$. It is seen that the maximum Volt-seconds are accumulated along the path $2-2'$

$$|\Delta \mathrm{Vs}|_{2-2'} = \left(\frac{-V_{DC}}{3} - \overline{v}_{cn}\right) \times \left(\frac{d_a - d_b}{f_{\mathrm{sw}}}\right) - \overline{v}_{cn}\left(\frac{1-d_a}{f_{\mathrm{sw}}}\right) \quad (13)$$

Performing a change of variable $\beta := \pi/3 - \alpha$ and substituting the voltages and the duty ratios for sector-I in the equation above yields the same expression as (11), but in terms of β. Similar result can be found for $\overline{v}_{cn} > -V_{DC}/3$ using the same change of variable. Therefore the ripple current of phase c in sector-I has the same envelope as phase a, but mirrored about $\alpha = \pi/6$.

E. Sectors-II–VI

The voltages synthesized by the inverter in (4) are rewritten with $\delta = 0$

$$\begin{aligned} \overline{v}_{an} &= mV_{DC}\cos(\alpha) \\ \overline{v}_{bn} &= mV_{DC}\cos(\alpha - 2\pi/3) \\ \overline{v}_{cn} &= mV_{DC}\cos(\alpha + 2\pi/3) \end{aligned} \quad (14)$$

Performing a change of variable $\theta := 2\pi/3 - \alpha$ yields

$$\begin{aligned} \overline{v}_{an} &= mV_{DC}\cos(\theta - 2\pi/3) \\ \overline{v}_{bn} &= mV_{DC}\cos(\theta) \\ \overline{v}_{cn} &= mV_{DC}\cos(\theta + 2\pi/3) \end{aligned} \quad (15)$$

In Sector-I, $\alpha \in [0, \pi/3)$; in Sector-II, $\alpha \in [\pi/3, 2\pi/3)$. As α varies between $\pi/3$ and $2\pi/3$, θ varies between $\pi/3$ and 0:

$$\begin{aligned} \overline{v}_{an}(\theta) &= \overline{v}_{bn}(\alpha) \\ \overline{v}_{bn}(\theta) &= \overline{v}_{an}(\alpha) \\ \overline{v}_{cn}(\theta) &= \overline{v}_{cn}(\alpha) \end{aligned} \quad (16)$$

Repeating the steps in the previous sections for Sector-II yields the same envelopes as (10)–(12) in terms of the angle θ: the envelope obtained from (10) applies to phase a in Sector-II

$$f(m,\alpha) := \max(|\Delta \mathrm{Vs}|)_{\overline{v}_{bn} \gtrless 0} = \frac{m}{\sqrt{3}} \cos\left(\alpha + \frac{\pi}{6}\right) + \frac{m}{2} \cos\left(\alpha - \frac{2\pi}{3}\right) - \frac{3}{2} m^2 \cos^2\left(\alpha - \frac{2\pi}{3}\right) \quad \text{Figs. 3(a),(b)} \quad (10)$$

$$g(m,\alpha) := \max(|\Delta \mathrm{Vs}|)_{\overline{v}_{an} > V_{DC}/3} = \frac{2}{\sqrt{3}} m \cos(\alpha + \pi/6) - \frac{m}{2} \cos(\alpha) + \frac{3}{2} m^2 \cos(\alpha) \cos\left(\alpha - \frac{2\pi}{3}\right) \quad \text{Fig. 3(c)} \quad (11)$$

$$h(m,\alpha) := \max(|\Delta \mathrm{Vs}|)_{\overline{v}_{an} < V_{DC}/3} = m \cos(\alpha) \left(\frac{1}{2} - m \cos(\alpha) - \frac{m}{2} \cos\left(\alpha - \frac{2\pi}{3}\right)\right) \quad \text{Fig. 3(d)} \quad (12)$$

whereas the ones obtained from (11) and (12) apply to phases b and c. Similar changes of variable establish the applicability of the result to all six sectors.

III. Simulation

The system of Fig. 1 was simulated with a $480\,\mathrm{V}, 60\,\mathrm{Hz}$ grid, $1\,\mathrm{mH}$ filter inductors, and $f_{\mathrm{sw}} = 6\,\mathrm{kHz}$. Fig. 5 shows the line currents at no-load for phases a, b along with the envelopes derived using (10)–(12). Fig. 6 shows all three line currents at no-load over a complete fundamental cycle and the derived envelope extended to all sectors. It is seen that the current is always confined within the derived envelope, and that the peak currents trace this envelope.

Since the three phases are symmetrical, the ripple currents' pattern alternates among the phases sector to sector. To establish a supremum, therefore, it is necessary to calculate the maxima of the functions f, g, h w.r.t. α as a function of the modulation index m.

IV. Upper limit as a function of m

A. Maximizing f

Let $\psi := \alpha - 2\pi/3$. Making the substitution in (10) and differentiating w.r.t. ψ,

$$f'_m(\psi) = -\frac{m}{\sqrt{3}} \sin\left(\psi + \frac{5\pi}{6}\right) - \frac{m}{2} \sin\psi + \frac{3}{2} m^2 \sin 2\psi \quad (17)$$

$$f''_m(\psi) = -\frac{m}{\sqrt{3}} \cos\left(\psi + \frac{5\pi}{6}\right) - \frac{m}{2} \cos\psi + 3m^2 \cos 2\psi \quad (18)$$

From (17) and (18), it is seen that $\psi = -\pi/2 (\equiv \alpha = \pi/6)$ is a maxima of (10) since $f'_m(-\pi/2) = 0, f''_m(-\pi/2) < 0$. Therefore,

$$\sup_{\alpha \in [0,\pi/3)} (f_m(\alpha)) = \frac{m}{2\sqrt{3}} \quad (19)$$

B. Maximizing h for $m < 1/3$

As discussed in II-B and II-C, the peak-to-peak ripple in the current of phase a at no-load in Sector-I is given by different expressions, depending upon the instantaneous value of $\overline{v}_{an}$. However, it is easy to see that for $m < 1/3$, the conditions for the applicability of $g(m,\alpha)$ to $\max(|\mathrm{Vs}|)$ would never be met since $\overline{v}_{an} < V_{DC}/3 \,\forall \alpha$

Therefore for lower modulation indexes $m < 1/3$, it is sufficient to maximize $h_m(\alpha)$ over $\alpha \in [0, \pi/3)$ to establish the supremum of phase a peak-to-peak current ripple. Fig. 7 shows the plot of $h'_m(\alpha)$ for different values of $m < 1/3$ and it is seen that the derivative h' is always less than or equal to zero for $m, \alpha \in [0, 1/3) \times [0, \pi/3)$: hence the supremum of phase a current ripple in Sector-I for $m < 1/3$ is $h_m(\alpha = 0)$

$$\sup_{\alpha \in [0,\pi/3)} (h_m(\alpha)) = \frac{m}{2}\left(1 - \frac{3m}{2}\right) \quad m < 1/3 \quad (20)$$

C. Phase a, $m \geq 1/3$

Let,

$$\alpha^* = \cos^{-1}\left(\frac{1}{3m}\right) \quad m \geq \frac{1}{3} \quad (21)$$

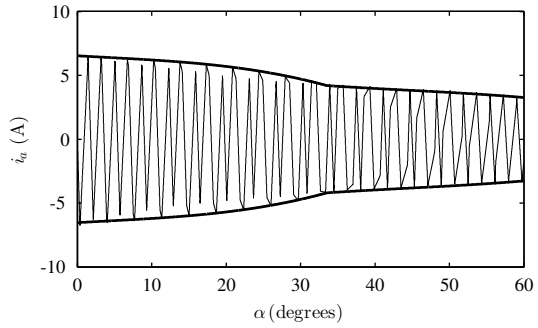

(a) Envelope of i_a at no-load derived from the functions $g(m,\alpha)$ (11) and $h(m,\alpha)$ (12)

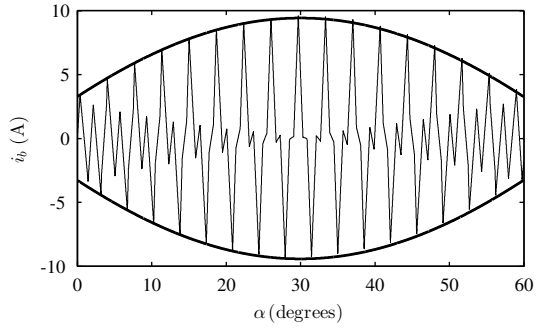

(b) Envelope of i_b at no-load derived from $f(m,\alpha)$ (10)

Fig. 5. Envelopes formed by the derived peak-to-peak currents in the first sector for phases a and b at $m = 0.40$

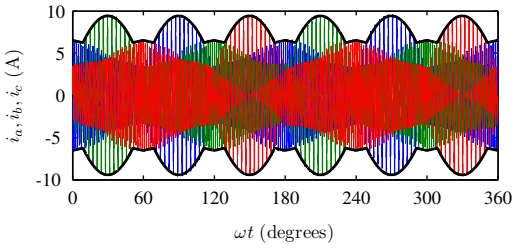

(a) i_a, i_b, i_c at no-load, $m = 0.40$

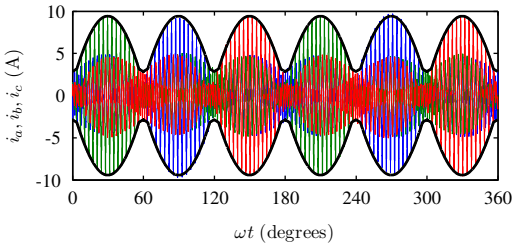

(b) i_a, i_b, i_c at no-load, $m = 0.55$

Fig. 6. Derived envelope and 3-phase currents for a complete fundamental cycle at no-load at different modulation indexes

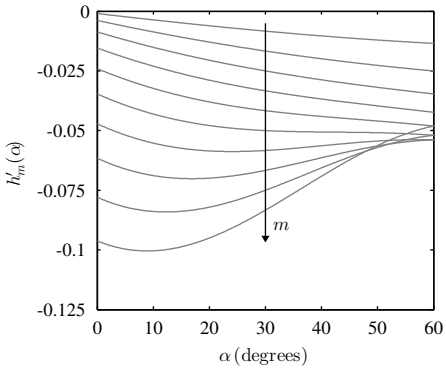

Fig. 7. The derivative of $h_m(\alpha)$ w.r.t. α for $m \in [0, 1/3)$

The envelope of i_a at no-load in Sector-I can be written as

$$\Gamma(m,\alpha) = \begin{cases} h_m(\alpha) & m < 1/3 \\ g_m(\alpha) & m, \alpha \in [1/3, 1/\sqrt{3}] \times [0, \alpha^*) \\ h_m(\alpha) & m, \alpha \in [1/3, 1/\sqrt{3}] \times [\alpha^*, \pi/3) \end{cases} \tag{22}$$

Fig. 8 is the surface plot of $m^{-1} \times \Gamma(m,\alpha)$ for $m, \alpha \in [1/3, 1/\sqrt{3}] \times [0, \pi/3)$, with the 'lid' being $m^{-1}\sup(f(\alpha))$ which is given by (19). The division by m is only for normalization. It is seen that the supremum of phase b peak-to-peak ripple current is also an upper bound on phase a current.

The supremum derived for phase b in (19) is a supremum for the peak-to-peak ripple current over the three phases for $m \geq 1/3$. For $m < 1/3$, the supremum is either given by (19), or by (20): it is further seen that the value given by (19) is greater than the value given by (20) not only for $m \geq 1/3$,

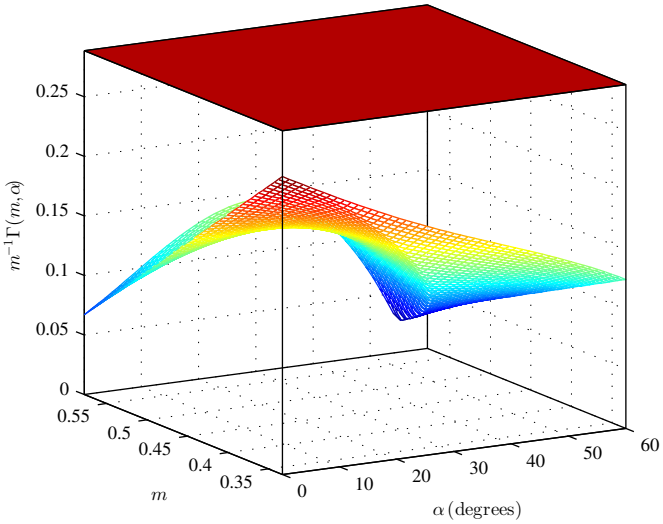

Fig. 8. $m^{-1}\Gamma(m,\alpha)$ and the $m^{-1}\sup_{\alpha\in[0,\pi/3)}(f(\alpha))$ plane for $m \in [1/3, 1/\sqrt{3}]$: it is seen that the supremum of f is also an upper bound of Γ for $m \in [1/3, 1/\sqrt{3}]$

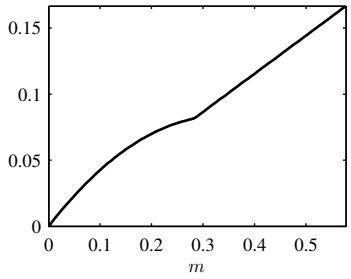

Fig. 9. The peak-to-peak current normalized by V_{DC}/Lf_{sw} as a function of the modulation index m

but for $m \geq m^*$ where $m^* = \frac{2}{3}\left(1 - \frac{1}{\sqrt{3}}\right)$

$$\tilde{i}_{\text{pp}} = \begin{cases} \dfrac{mV_{DC}}{2Lf_{\text{sw}}}\left(1 - \dfrac{3m}{2}\right) & m \in [0, m^*) \\ \dfrac{mV_{DC}}{2\sqrt{3}Lf_{\text{sw}}} & m \in [m^*, 1/\sqrt{3}] \end{cases} \tag{23}$$

The normalized peak-to-peak current as a function of m from (23) is plotted in Fig. 9.

Further, as argued in II-D, for Sector-I, the upper bound on phase a current ripple is also an upper bound on phase c current ripple. In addition, as explained in II-E, considering one sector is sufficient to predict the envelope of the ripple currents in all sectors. Moreover, the ripple current analysis, although conducted at no-load, is valid at load as well since the high-frequency components in the inverter output voltage that cause the ripple current to flow are present at all loads, including no-load. Therefore, the preceding analysis for phases a, b in Sector-I establishes the supremum on the ripple currents of *all* three phases in *all* six sectors, at *all* loading conditions.

V. Conclusion

This paper presented an analysis of the high-frequency switching current ripple in the output ac current of a two-level voltage source inverter connected to the grid using filter inductors. The envelope of the ripple current was derived analytically for one sector and its applicability to all sectors was shown. The results were verified using simulation and a supremum of the peak-to-peak ripple current was established. This upper limit on ripple current is essential for proper filter design to meet the grid current THD criteria.

Validity of the analysis to LCL filter was claimed qualitatively. Examination using simulation and hardware prototype is underway.

References

[1] W. Wu, Y. Sun, M. Huang, X. Wang, H. Wang, F. Blaabjerg, M. Liserre, and H.-h. Chung, "A robust passive damping method for llcl-filter-based grid-tied inverters to minimize the effect of grid harmonic voltages," *Power Electronics, IEEE Transactions on*, vol. 29, no. 7, pp. 3279–3289, July 2014.

[2] W. Wu, Y. He, and F. Blaabjerg, "An llcl power filter for single-phase grid-tied inverter," *Power Electronics, IEEE Transactions on*, vol. 27, no. 2, pp. 782–789, Feb 2012.

[3] D. G. Holmes and T. A. Lipo, *Pulse width modulation for power converters: principles and practice*. John Wiley & Sons, 2003, vol. 18.

[4] K. Jalili and S. Bernet, "Design of lcl filters of active-front-end two-level voltage-source converters," *Industrial Electronics, IEEE Transactions on*, vol. 56, no. 5, pp. 1674–1689, May 2009.

[5] S. Bernet, S. Ponnaluri, and R. Teichmann, "Design and loss comparison of matrix converters, and voltage-source converters for modern ac drives," *Industrial Electronics, IEEE Transactions on*, vol. 49, no. 2, pp. 304–314, Apr 2002.